Jilin Daxue Xuebao (Gongxueban)/Journal of Jilin University (Engineering and Technology Edition)
ISSN: 1671-5497
E-Publication: Online Open Access
Vol: 42 Issue: 10-2023
DOI: 10.5281/zenodo.10060151

AN ASSESSMENT OF THE RELATIONSHIP BETWEEN POPULATION DENSITY AND THE INCIDENCE OF DENGUE HEMORRHAGIC FEVER

THI-TUYET-MAI NGUYEN*
Faculty of Pharmacy, East Asia University of Technology, Hanoi, Vietnam.
*Corresponding Author Email: maintt@eaut.edu.vn

HUONG-GIANG NGUYEN
Faculty of Pharmacy, East Asia University of Technology, Hanoi, Vietnam.

THI-QUYNH NGUYEN
Faculty of Nursing, East Asia University of Technology, Hanoi, Vietnam.

1. INTRODUCTION

Dengue, including dengue fever and dengue haemorrhagic fever, is the most rapidly spreading mosquito-borne viral disease and an increasing public health problem globally (1). During the past 50 years, the incidence of dengue has increased by 30 fold, parallel with the increasing geographic expansion from urban to rural areas (2,3). According to current estimates, at least 100 countries are endemic of dengue and about 2.5 billion people are at risk in tropical and subtropical regions, with about 50 million dengue infections occurring annually (1). The revised International Health Regulations 2005 included dengue as a disease that may constitute a public health emergency of international concern with implications for health security due to disruption and rapid epidemic spread beyond national borders (4). The impact of global warming on human health, especially in vector-borne diseases, is increasingly becoming a public health concern, because the risk of dengue has been reported to be associated directly or indirectly with seasonal changes in climate (2,3,5,6), and mosquito larval indices (7–9).

GIS and spatial statistics have been widely applied on infectious disease mapping such as mapping the COVID-19 pandemic (10–12), hand-foot-and-mouth disease (13,14) and dengue fever/dengue hemorrhagic fever (15–17). For instance, in the study of COVID-19, a spatio-temporal analysis and hotspots detection of COVID-19 in southern, northern and western Europe was carried out using spatial statistics (18). In Oman, local Moran's I autocorrelation coefficient, Getis-Ord General-G high/low clustering, and Getis-Ord Getis-Ord's G_i^* statistic were successfully emloyed to study spatio-temporal COVID-19 spread (19). To determine the effects of living environment deprivation, an assessment of the COVID-19 hotspots in Kolkata, India was carried out utilizing the Getis-Ord G statistic and regionally weighted principal component analysis (20). Exploratory spatial data analysis and the geodetector approach were also used to analyze the regional and temporal differentiation characteristics and the contributing elements that influenced the COVID-19 epidemic spread in mainland China (21).

A part from these countries, GIS and spatial statistics have also been successfully used in COVID-19 studies in other countries such as the United States (22), England (23),

Jilin Daxue Xuebao (Gongxueban)/Journal of Jilin University (Engineering and Technology Edition)
ISSN: 1671-5497
E-Publication: Online Open Access
Vol: 42 Issue: 10-2023
DOI: 10.5281/zenodo.10060151

Spain (24) and Italy (25). In the study of hand-foot-and-mouth disease, a study on spatio-temporal distribution and hotspots of hand-foot-and-mouth disease was successfully carried out in northern Thailand (26). In China, spatial clustering and changing trend of hand-foot-mouth disease were identified during 2008-2011 (27). In 2014, anothe study has been conducted for a temporal and spatial mapping of HFMD that covered 13 all divisions of Sarawak during 2006 - 2012 (28). In studies of dengue, geographic information systems (GIS) have mapped the regional clustering patterns of dengue cases and examined the relationships between these patterns and pertinent entomological parameters (15–17) and environmental conditions (29), and have determined the dengue and vector distributions' spatial-temporal diffusion patterns (17,30).

This study aims to assess the relationship between population density and dengue hemorrhagic fever in August 2023 in Ho Chi Minh city. The first step of this method will use Exploratory data analysis (EDA) techniques to investigate the distribution patterns of DHF incidence. It will go on to use Getis Ord statistic to detect hotspots and coldspots of DHF infection rates. A scatter plot will be then employed to quantitatively assess the relationship between population density and DHF infection rates and Getis Ord statistics. Finally, the last section will focus on the main findings of the study.

2. DATA USED AND METHODS

2.1 Data used

In Vietnam, dengue is highly prevalent, and the incidence rate is reported to be 145/100,000 population according to the national surveillance system data from 2010 (31). All four dengue serotypes circulate (32). Vietnam seems to follow similar trends to Thailand where dengue epidemiology has been studied extensively. Despite mosquito control efforts, dengue fever/dengue hemorrhagic fever (DF/DHF) has steadily increased in both incidence and range of distribution in Thailand, and the incidence rate in 2010 was reported to be 177/100,000 population (31).

Dengue has now spread to all provinces, districts, sub-districts and communities, and is seen every year (33). Recently, comparing with those reported in July, 350 cases of dengue fever were recorded, an increase of 19.1 percent compared to the average of 4 weeks ago. From the beginning of the year to August 19, a total of 10,847 DHF cases were recorded. In this study, a dataset of DHF infection rates reported in August 2023 in Ho Chi Minh city was used to assess the relationship between population density and dengue hemorrhagic fever.

2.2 Methods

Exploratory data analysis.

Exploratory data analysis (EDA) involves the use of statistical techniques to identify patterns that may be hidden in a group of numbers. Two of these techniques is the "box plot" and " scatter plot" which is used to visually summarize and compare groups of data. The box plot uses the median, the approximate quartiles, and the lowest and highest data points to convey the level, spread, and symmetry of a distribution of data values (34).

Jilin Daxue Xuebao (Gongxueban)/Journal of Jilin University (Engineering and Technology Edition)
ISSN: 1671-5497
E-Publication: Online Open Access
Vol: 42 Issue: 10-2023
DOI: 10.5281/zenodo.10060151

The box plot is one of a diverse family of statistical techniques, called exploratory data analysis, used to visually identify patterns that may otherwise be hidden in a data set. Three useful proper ties of exploratory data analysis techniques are that they require few prior assumptions about the data, their statistical measures are resistant to outlying data values that may inordinately influence an analysis, and they emphasize visual displays that clearly highlight important landmarks of the data. Lines that extend from the box (either up or down) are called whiskers.

Lower whiskers indicate lower values of the data group that are within the *IQR*. Upper whiskers indicate higher values from the data group that are within the *IQR*. Whisker length, $1.5 * IQR$, starts from the end of the *IQR* box, and ends at data values that are not categorized as outliers (as shown in the Figure 1, the boundaries are the *UIF* and *LIF* lines). Thus, the largest and smallest values of the observed data (excluding outliers) are still part of the Boxplot which is located right at the end of the whiskers edge line.

$$IQR = Q_3 - Q_1 \quad (1)$$

$$LIF = Q_1 - 1.5 * IQR \quad (2)$$

$$UIF = Q_3 + 1.5 * IQR \quad (3)$$

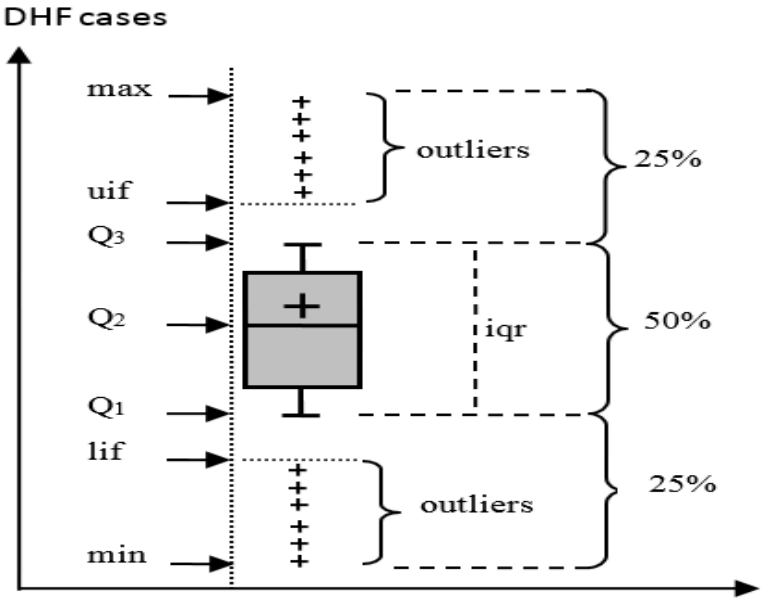

Figure 1: Boxpot

*(Notes: min - smallest observation value, max - the largest observation value; uif – Upper Inner Fence; Q_3 - highest quartile or third quartile; Q_2 - **median** or middle value; Q_1 - lowest quartile or first quartile; iqr-Inner Quatile Range; lif - Lower Inner Fence).*

A scatter plot is a type of plot or mathematical diagram using Cartesian coordinates to display values for typically two variables for a set of data (35). If the points are coded, one additional variable can be displayed. The data are displayed as a collection of points, each having the value of one variable determining the position on the horizontal axis and

Jilin Daxue Xuebao (Gongxueban)/Journal of Jilin University (Engineering and Technology Edition)
ISSN: 1671-5497
E-Publication: Online Open Access
Vol: 42 Issue: 10-2023
DOI: 10.5281/zenodo.10060151

the value of the other variable determining the position on the vertical axis (36). A scatter plot can be used either when one continuous variable is under the control of the experimenter and the other depends on it or when both continuous variables are independent. If a parameter exists that is systematically incremented and/or decremented by the other, it is called the control parameter or independent variable and is customarily plotted along the horizontal axis. The measured or dependent variable is customarily plotted along the vertical axis. If no dependent variable exists, either type of variable can be plotted on either axis and a scatter plot will illustrate only the degree of correlation (not causation) between two variables. A scatter plot can suggest various kinds of correlations between variables with a certain confidence interval. Correlations may be positive (rising), negative (falling), or null (uncorrelated).

Hotspot analysis

There are different methods for analyzing spatial patterns and detecting hotspots including spatial autocorrelation and cluster analysis (37). A hotspot can be defined as an area that has higher concentration of events compared to the expected number given a random distribution of events (38). The application of hotspot analysis within public health and epidemiological research as well as in other disciplines (e.g., a great deal of the literature on hotspot analysis comes from crime mapping and research) has increased significantly in the past couple of decades mainly due to the advent of Geographic Information Systems (GIS)-based software (39–41).

Spatial autocorrelation analysis looks at how similar are those values that are closer to each other (42). Measures of spatial autocorrelation can be categorized as global or local indicators of spatial association (43). Spatial autocorrelation analysis was performed on the incidence rates to test whether the cases were distributed randomly over space and, if not, to evaluate any identified spatial disease clusters for statistical significance (44). A hotspot is defined as a condition indicating some form of clustering in a spatial distribution (44). Hotspot analysis is based on the *Getis-Ord's* G_i^* statistic. Hotspot analysis characterizes the presence of hotspots (high clustered values) and coldspots (low clustered values) over an entire area by looking at each feature within the context of its neighboring features (38). Hotspot can separate clusters of high values from cluster of low values. It is, therefore, *Getis-Ord's* G_i^* statistic was used to identify the counties of high and low numbers of COVID-19 cases (45,46). The form of *Getis-Ord's* G_i^* statistic is defined as follows (47):

$$G_i^* = \frac{\sum_{j=1}^{N} W_{ij}\, x_j - \overline{x} \sum_{j=1}^{N} W_{ij}}{S \sqrt{\frac{N \sum_{j=1}^{N} [W_{ij}^2 - (W_{ij})^2]}{N-1}}} \qquad (4)$$

with:

$$\overline{x} = \frac{1}{N} \sum_{j=1}^{N} x_j \qquad (5)$$

Jilin Daxue Xuebao (Gongxueban)/Journal of Jilin University (Engineering and Technology Edition)
ISSN: 1671-5497
E-Publication: Online Open Access
Vol: 42 Issue: 10-2023
DOI: 10.5281/zenodo.10060151

and:

$$S = \sqrt{\frac{\sum_{j=1}^{N} x_j^2}{N} - (\overline{x})^2} \qquad (6)$$

Expectation:

$$\mathrm{E}(\mathrm{G}_\mathrm{i}^*) = \frac{\mathrm{W}_i^*}{\mathrm{n}-1} \qquad (7)$$

with:

$$\mathrm{W}_i^* = \sum_{j=1}^{\mathrm{n}} \mathrm{w}_{ij}(d) \qquad (8)$$

and variance:

$$\mathrm{Var}(\mathrm{G}_\mathrm{i}^*) = \frac{\mathrm{W}_i^*(\mathrm{n}-\mathrm{W}_i^*)\mathrm{Y}_{i2}^*}{\mathrm{n}^2(\mathrm{n}-1)(\mathrm{Y}_{i1}^*)^2} \qquad (9)$$

with:

$$\mathrm{Y}_{i1}^* = \frac{\sum_{j=1}^{\mathrm{n}} \mathrm{x_j}}{\mathrm{n}}; \qquad (10)$$

and:

$$\mathrm{Y}_{i2}^* = \frac{\sum_{i=1}^{\mathrm{n}} \sum_{j=1}^{\mathrm{n}} \left(\mathrm{x_i x_j}\right)^2}{\mathrm{n}} - (\mathrm{Y}_{i1}^*)^2; \qquad (11)$$

where: the *Getis-Ord's* G_i^* statistic is computed for the number of COVID-19 cases at county *i*; x_i, x_j, $\bar{x}$, and W_{ij} are defined in equation (1); and N is the total number of neighborhood counties as defined in equation (2). W_{ij} can be constructed using the methods of the first order and second of contiguity. In this study, adjacency to compute W_{ij} is defined using the first order of continuity.

The *Getis-Ord's* G_i^* coefficient at county *i* (G_i^*) also ranges between -1 and +1. If $G_i^* > 0$ and $p(G_i^*) < \alpha$ then there exists a spatial clustering of high-high values (45,46). In this case, these high-high values, so-called a hotspots, reflects the presence of high numbers of COVID-19 cases among county *i* and its neighborhood counties ($j \in J_i$). Whereas, if $G_i^* < 0$ and $p(G_i^*) < \alpha$ then there exists a spatial clustering of low-low values (45,46). These low-low values are called a coldspots indicating low numbers of COVID-19 cases among county *i* and its neighborhood counties ($j \in J_i$). Similar to those in the definition of local Moran's I statistic, if the value of G_i^*close zero and $p(G_i^*) < \alpha$ then there will be neither hotspots nor coldspots or random distribution of COVID-19 cases (46). Clusters of cases that occur randomly can also have an influence on the spread of an infectious disease (44). The output from *Getis-Ord's* G_i^* statistic identifies spatial clusters of high values (hotspots) and spatial clusters of low values (cold spots).

Jilin Daxue Xuebao (Gongxueban)/Journal of Jilin University (Engineering and Technology Edition)
ISSN: 1671-5497
E-Publication: Online Open Access
Vol: 42 Issue: 10-2023
DOI: 10.5281/zenodo.10060151

The high/low clustering tool is an inferential statistic, which means that the results of the analysis are interpreted within the context of a null hypothesis (44). A lots of attempts have been put on the use of *Getis-Ord's* G_i^* statistic with the help of ArcGIS software using *Getis z-scores* (21,38,48) defined in a study by Mitchel (48). The presence of a strongly skewed distribution in the dataset fails the test. It is, therefore, testing for the significance of the *Getis-Ord's* G_i^* statistic in this study was also carried out by a randomization test using 999 permutations. In this work, with the help of the spatial statistics software, GeoDA, developed by (49), a randomization test was used to test the significance of spatial autocorrelation statistics. Spatial auto-correlation statistics were generated and tested at the significance of 0.05 using 999 permutations. When the p-value is very small, it means it is very unlikely (small probability) that the observed spatial pattern is the result of random processes, so the null hypothesis can be rejected (44).

Pearson Correlation Analysis

In statistics, the Pearson correlation coefficient is a correlation coefficient that measures linear correlation between two sets of data. It is the ratio between the covariance of two variables and the product of their standard deviations; thus, it is essentially a normalized measurement of the covariance, such that the result always has a value between -1 and 1. It assigns a value between -1 and 1, where 0 is no correlation, 1 is total positive correlation, and -1 is total negative correlation. As with covariance itself, the measure can only reflect a linear correlation of variables, and ignores many other types of relationships or correlations.

$$r = \frac{\sum_{i=1}^{n}(x_i - \overline{x})(y_i - \overline{y})}{\sqrt{\sum_{i=1}^{n}(x_i - \overline{x})^2 (y_i - \overline{y})^2}} \qquad (12)$$

3. RESULTS AND DISCUSSIONS

3.1 Distribution of DHF incidence and population density

Data on statistical indicators of DHF infection rate and population density were statistically summarized in Table 1. Data from Table 1 shows that, in August 2023, the lowest and highest DHF infection rates were 5 cases100,000 people and 28 cases/100,000 people, respectively. The vaues of the mean and the median of DHF infection rates were 16.1/100,000 people and 15.5 cases/100,000 people, respectively. In which the data dispersion of DHF infection rates determined by IQR and SDEV were 8 cases/100,000 people and 6.1 cases/100,000 people, respectively. Meanwhile, the lowest and highest population density were 106 people/km^2 and 65,113 people/km^2, respectively. The values of the mean and the median population density were 24,611 people/km^2 and 23,581 people/km^2, respectively. In which the dispersion of the population density determined with IQR and SDEV was 32,243 people/km^2 and 19,914 people/km^2, respectively.

The distribution of DHF infection rates in August 2023 and population density were shown in the boxplot as shown in Figure 2 left and right, respectively. Data from Figure 2 shows that the boxplot was slightly skewed to the top (skewed to the direction of the larger values). This is consistent with those obtained in Table 1 where the mean value was

Jilin Daxue Xuebao (Gongxueban)/Journal of Jilin University (Engineering and Technology Edition)
ISSN: 1671-5497
E-Publication: Online Open Access
Vol: 42 Issue: 10-2023
DOI: 10.5281/zenodo.10060151

larger than the median value. This proves that the high DHF infection rate and high population density were more prominent throughout Ho Chi Minh City.

Table 1: Statistical Descriptives For Dhf Incidence And Population Density.

Variables	Statistical descriptives							
	Min	Mean	Median	Max	Q1	Q3	IQR	SDEV
DHF incidence	5	16.1	15.5	28	11	19	8	6.1
Population density	106	24.611	23.581	65.113	5.149	37.392	32.243	19.914

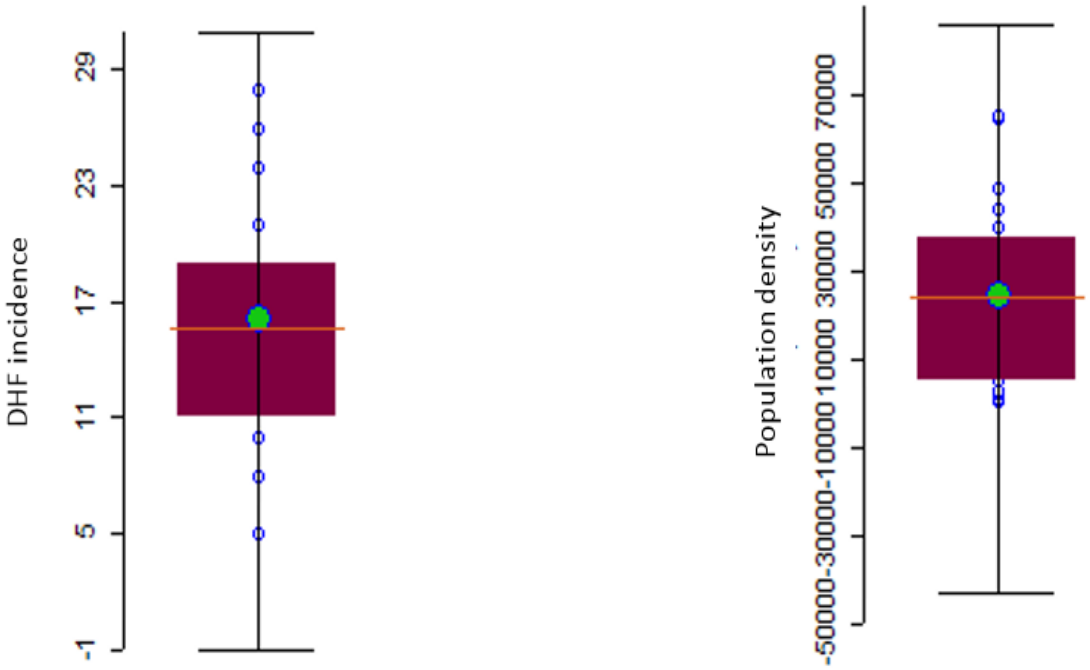

Fig 2: Boxplots of DHF incidence (left) and population density (right).

The spatial distribution of DHF incidence in August of 2023 and population density was shown in the maps in Figure 3 left and right, respectively. Data from Figure 3 (left) shows that high DHF infection rates mainly appeared in districts near the city center, whereas low DHF infection rates were mainly distributed in a few districts in the centre of the city, and som suburban districts in the north and south of the city. It can be seen clearly that the closer to the city center, the higher the DHF infection rate. Some districts had high and very high infection rates such as Nha Be (28 cases/100,000 people), District 1 (26 cases/100,000 people), District 7 (24 cases/100,000 people), Tan Phu (24 cases/100,000 people) and Binh Thanh (21 cases/100,000 people), whereas some districts had low infection rates such as Can Gio (5 cases/100,000 people), District 6 and District 11 (8 cases/100,000 people), and Phu Nhuan (10 cases/100,000 people). Meanwhile, the spatial distribution of population density was shown in Figure 3 (right). Data from Figure 3 illustrate that high population density was mainly concentrated in urban districts in the city center. Some districts with high population density were District 10 (65,114 people/km^2), District 11 (64,696 people/km^2), District 4 (48,579 people/km^2) and District

Jilin Daxue Xuebao (Gongxueban)/Journal of Jilin University (Engineering and Technology Edition)
ISSN: 1671-5497
E-Publication: Online Open Access
Vol: 42 Issue: 10-2023
DOI: 10.5281/zenodo.10060151

5 (43,913 people/km^2). Low population density was mainly distributed in the northern, southern, eastern and western suburban districts surrounding the city center. Low population density were found in some suburban districts such as Can Gio (106.5 people/km^2), Cu Chi (926.5 people/km^2), Nha Be (2239 people/km^2) and Binh Chanh (2687 people/km^2).

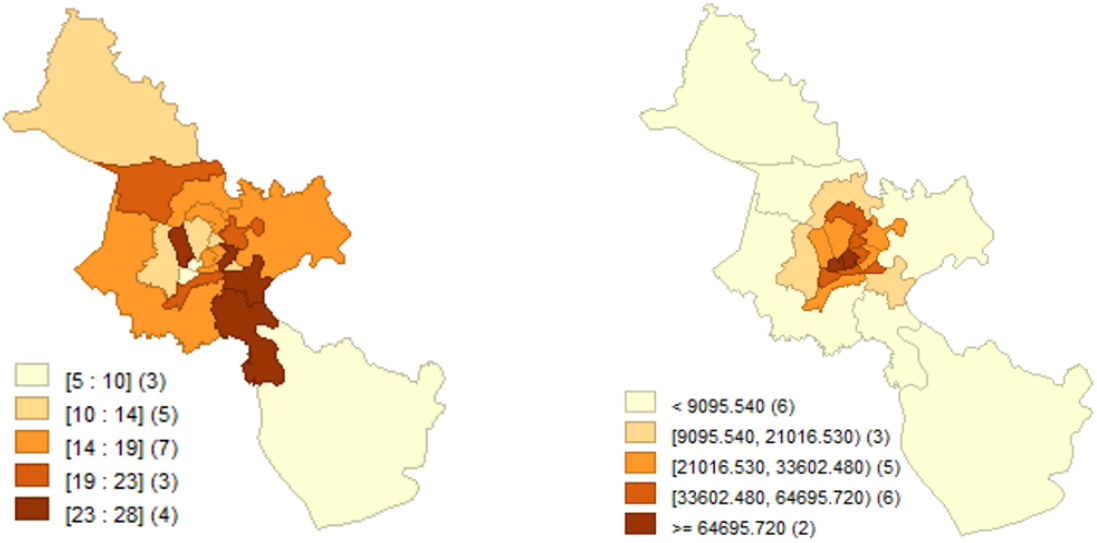

Fig 3: Equal interval maps of DHF incidence (left) and population density (right).

3.2 Analysis of DHF hotspots

The distribution of Getis Ord statistic obtained from DHF infection rates were shown in Figure 4. Data from Figure 4 (left) shows that the high values of Getis Ord coefficients was mainly concentrated in the east and west of the city. Meanwhile, low values of Getis Ord statistics were found in the northern and southern suburban districts and some urban districts in the city center. In August, Getis Ord's statistic successfully detected three hotspots and one coldspot. Three hotspots of DHF were discovered in the west and south of the city in the districts of District 4 (11 cases/100,000 people), Binh Chanh (16 cases/100,000 people), Can Gio (5 cases/100,000 people). Meanwhile, a coldspot was also detected in Tan Phu (24 cases/100,000 people), a district in the city center.

Data in boxplots in Figure 4 (right) demonstrates that the Getis Ord statistics were skewed to the upward. This proves that the Getis Ord statistic was skewed to the side where many high number of DHF cases were detected. It was found that the lowest and highest values of the Getis Ord statistic were 0.039 and 0.056, respectively. The mean and median values of Getis Ord statistic were 0.047 and 0.046, respectively. In which the data dispersion of the Getis Ord statistic determined by IQR and SDEV was 0.007 and 0.005 respectively. Data in Figure 4 shows that high values of Getis Ord statistics were found in some districts including Binh Chanh (0.0563), District 7 (0.0545), District 4 (0.054), Thu Duc (0.054) and Nha Be (0.051). High values of Getis Ord statistic were mainly found in districts in western and eastern areas of the city. Meanwhile, low values of Getis Ord

Jilin Daxue Xuebao (Gongxueban)/Journal of Jilin University (Engineering and Technology Edition)
ISSN: 1671-5497
E-Publication: Online Open Access
Vol: 42 Issue: 10-2023
DOI: 10.5281/zenodo.10060151

statistic were mainly detected in districts of Tan Phu (0.0389), District 11 (0.041), Tan Binh (0.041), and District 6 (0.042).

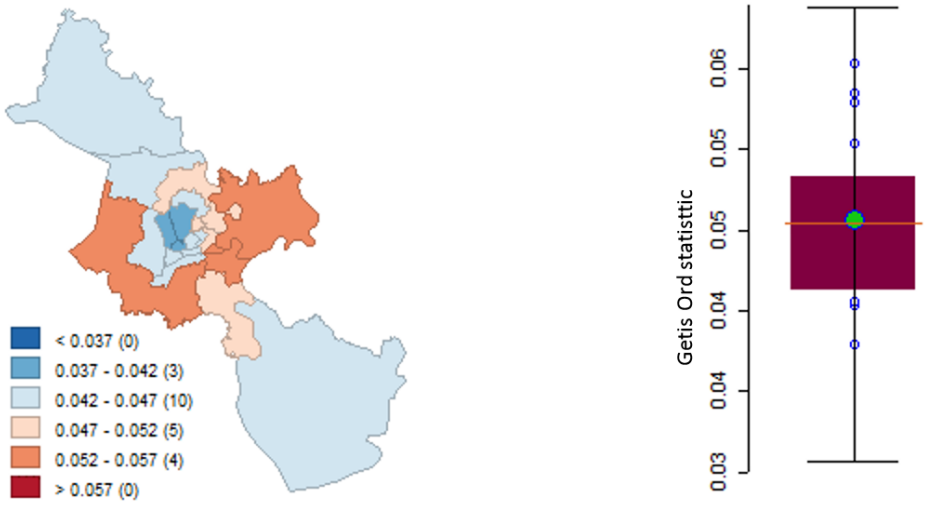

Fig 4: Distribution of Getis Ord's statistic: (a) boxmap and (b) boxplot.

3.3 Analysis of the relationship between population density and DHF infection rate

As discussed above, a scatterplot is a type of data display that shows the relationship between two numerical variables. In this study, the relationship between population density and DHF infection rates and Getis Ord statistic in Ho Chi Minh city was investigated using the scatter plot. Data from the scatter plot in Figure 5 demonstrate the relationship between population density and DHF infection rates and Getis Ord statistic. It can be seen that there was a negative correlation between population density and both variables (DHF infection rates and Getis Ord statistic). It can be concluded that as population density increases, the DHF infection rate tends to decrease in August.

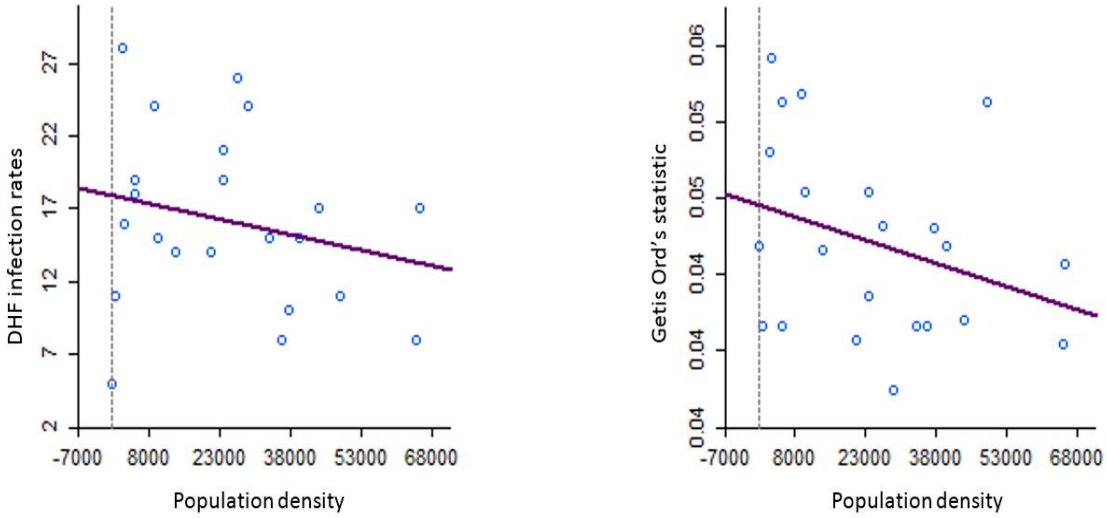

Fig 5: Scatterplot of population density against DHF infection rates (left) and Getis Ord's statistic.

Jilin Daxue Xuebao (Gongxueban)/Journal of Jilin University (Engineering and Technology Edition)
ISSN: 1671-5497
E-Publication: Online Open Access
Vol: 42 Issue: 10-2023
DOI: 10.5281/zenodo.10060151

4. CONCLUSIONS

Dengue fever is one of the most prevalent arboviral diseases in the world, and its global range of transmission has increased significantly in recent decades. This study is set out to assess the relationship between population density and dengue hemorrhagic fever in August of 2023 in Ho Chi Minh city, Vietnam. EDA techniques were first used to investigate the distribution patterns of DHF incidence. Getis Ord statistic was then employed to detect hotspots and coldspots of DHF infection rates. A scatter plot was then employed to quantitatively assess the relationship between population density and DHF infection rates and Getis Ord statistic. Finally, a dataset of DHF cases recorded in August 2023 in Ho Chi Minh city was used to illustrate the proposed methods. It was found that there existed a negative correlation between population density and both of DHF infection rates and Getis Ord statistic. The population density likely decreases dengue hemorrhagic fever infection rates in August of 2023 in Ho Chi Minh city. It can be concluded that spatial statistics and EDA have proved their effectiveness in the assessment of the relationship between population density and the incidence of dengue hemorrhagic fever. Findings of this study not only provide an insight into the effects of population density on DHF infection rates, but also helps to understand different socio-ecological drivers of locally or overseas acquired dengue hemorrhagic fever.

Acknowledgement

The authors would like to thank HCDC for providing the data. The authors acknowledge the editors and anonymous reviewers for their insightful criticism and recommendations on this manuscript which helped to greatly improve the quality of the paper.

References

1) Organization WH, Research SP for, Diseases T in T, Diseases WHOD of C of NT, Epidemic WHO, Alert P. Dengue: guidelines for diagnosis, treatment, prevention and control. World Health Organization; 2009.
2) Hales S, De Wet N, Maindonald J, Woodward A. Potential effect of population and climate changes on global distribution of dengue fever: an empirical model. Lancet. 2002;360(9336):830–4.
3) Russell RC. Mosquito-borne disease and climate change in Australia: time for a reality check. Aust J Entomol. 2009;48(1):1–7.
4) Organization WH. Revision of the International Health Regulations, 2005. Elektron erişim Adres http//www who int/csr/ihr/en/index html. 2005;
5) Hu W, Clements A, Williams G, Tong S. Dengue fever and El Nino/Southern Oscillation in Queensland, Australia: a time series predictive model. Occup Environ Med. 2010;67(5):307–11.
6) Organization WH. Using climate to predict infectious disease epidemics. 2005;
7) Arunachalam N, Tana S, Espino FE, Kittayapong P, Abeyewickrem W, Wai KT, et al. Eco-bio-social determinants of dengue vector breeding: a multicountry study in urban and

ISSN: 1671-5497
E-Publication: Online Open Access
Vol: 42 Issue: 10-2023
DOI: 10.5281/zenodo.10060151

periurban Asia. Bull World Health Organ. 2010;88(3):173–84.

8) Hales S, Weinstein P, Souares Y, Woodward A. El Niño and the dynamics of vectorborne disease transmission. Environ Health Perspect. 1999;107(2):99–102.

9) Gürtler RE, Garelli FM, Coto HD. Effects of a five-year citywide intervention program to control Aedes aegypti and prevent dengue outbreaks in northern Argentina. PLoS Negl Trop Dis. 2009;3(4):e427.

10) Shadeed S, Alawna S. GIS-based COVID-19 vulnerability mapping in the West Bank, Palestine. Int J Disaster Risk Reduct. 2021;64:102483.

11) Kamel Boulos MN, Geraghty EM. Geographical tracking and mapping of coronavirus disease COVID-19/severe acute respiratory syndrome coronavirus 2 (SARS-CoV-2) epidemic and associated events around the world: how 21st century GIS technologies are supporting the global fight against outbr. Vol. 19, International journal of health geographics. Springer; 2020. p. 1–12.

12) Utomo IC, Fadlilah U. Mapping of Covid-19 Vaccination Recipients in Sukoharjo Regency Based on Webgis. J Tek Inform. 2022;3(6):1773–81.

13) Nguyen HX, Chu C, Nguyen HLT, Nguyen HT, Do CM, Rutherford S, et al. Temporal and spatial analysis of hand, foot, and mouth disease in relation to climate factors: a study in the Mekong Delta region, Vietnam. Sci Total Environ. 2017;581:766–72.

14) Deng T, Huang Y, Yu S, Gu J, Huang C, Xiao G, et al. Spatial-temporal clusters and risk factors of hand, foot, and mouth disease at the district level in Guangdong Province, China. PLoS One. 2013;8(2):e56943.

15) Ali M, Wagatsuma Y, Emch M, Breiman RF. Use of a geographic information system for defining spatial risk for dengue transmission in Bangladesh: role for Aedes albopictus in an urban outbreak. Am J Trop Med Hyg. 2003;69(6):634–40.

16) Tran A, Deparis X, Dussart P, Morvan J, Rabarison P, Remy F, et al. Dengue spatial and temporal patterns, French Guiana, 2001. Emerg Infect Dis. 2004;10(4):615.

17) Morrison AC, Getis A, Santiago M, Rigau-Perez JG, Reiter P. Exploratory space-time analysis of reported dengue cases during an outbreak in Florida, Puerto Rico, 1991-1992. Am J Trop Med Hyg. 1998;58(3):287–98.

18) Shariati M, Mesgari T, Kasraee M, Jahangiri-Rad M. Spatiotemporal analysis and hotspots detection of COVID-19 using geographic information system (March and April, 2020). J Environ Heal Sci Eng. 2020;18:1499–507.

19) Al-Kindi KM, Alkharusi A, Alshukaili D, Al Nasiri N, Al-Awadhi T, Charabi Y, et al. Spatiotemporal assessment of COVID-19 spread over Oman using GIS techniques. Earth Syst Environ. 2020;4:797–811.

20) Das A, Ghosh S, Das K, Basu T, Dutta I, Das M. Living environment matters: Unravelling the spatial clustering of COVID-19 hotspots in Kolkata megacity, India. Sustain Cities Soc. 2021;65:102577.

21) Alves JD, Abade AS, Peres WP, Borges JE, Santos SM, Scholze AR. Impact of COVID-19 on the indigenous population of Brazil: A geo-epidemiological study. Epidemiol Infect. 2021;149:e185.

22) Liu L, Hu T, Bao S, Wu H, Peng Z, Wang R. The spatiotemporal interaction effect of COVID-19 transmission in the United States. ISPRS Int J Geo-Information. 2021;10(6):387.

23) Huangfu P, Atkinson R. Long-term exposure to NO2 and O3 and all-cause and respiratory

ISSN: 1671-5497
E-Publication: Online Open Access
Vol: 42 Issue: 10-2023
DOI: 10.5281/zenodo.10060151

mortality: A systematic review and meta-analysis. Environ Int. 2020;144:105998.

24) Belvis F, Aleta A, Padilla-Pozo Á, Pericàs J-M, Fernández-Gracia J, Rodríguez JP, et al. Key epidemiological indicators and spatial autocorrelation patterns across five waves of COVID-19 in Catalonia. Sci Rep. 2023;13(1):1–11.

25) Ghosh P, Cartone A. A Spatio-temporal analysis of COVID-19 outbreak in Italy. Reg Sci Policy Pract. 2020;12(6):1047–62.

26) Samphutthanon R, Kumar Tripathi N, Ninsawat S, Duboz R. Spatio-temporal distribution and hotspots of hand, foot and mouth disease (HFMD) in northern Thailand. Int J Environ Res Public Health. 2014;11(1):312–36.

27) Xiao G, Hu Y, Ma JQ, Hao YT, Wang XF, Zhang YJ, et al. Spatial clustering and changing trend of hand-foot-mouth disease during 2008-2011 in China. Zhonghua liu xing bing xue za zhi= Zhonghua liuxingbingxue zazhi. 2012;33(8):808–12.

28) Sham NM, Krishnarajah I, Ibrahim NA, Lye M-S. Temporal and spatial mapping of hand, foot and mouth disease in Sarawak, Malaysia. Geospat Health. 2014;8(2):503–7.

29) Bohra A, Andrianasolo H. Application of GIS in Modeling Dengue Risk Based on Sociocultural Data: Case of Jalore, Rajasthan, India. 2001;

30) Ungchusak K, Burke DS. Travelling waves in the occurrence of dengue hemorrhagic fever in thailand. Nature. 2004;427:344347Cushing.

31) Lee J-S, Mogasale V, Lim JK, Carabali M, Sirivichayakul C, Anh DD, et al. Correction: A Multi-country Study of the Household Willingness-to-Pay for Dengue Vaccines: Household Surveys in Vietnam, Thailand, and Colombia. PLoS Negl Trop Dis. 2015;9(9):e0004070.

32) Tien NTK, Luxemburger C, Toan NT, Pollissard-Gadroy L, Huong VTQ, Van Be P, et al. A prospective cohort study of dengue infection in schoolchildren in Long Xuyen, Viet Nam. Trans R Soc Trop Med Hyg. 2010;104(9):592–600.

33) Burke DS, Nisalak A, Johnson DE, Scott RM. A prospective study of dengue infections in Bangkok. Am J Trop Med Hyg. 1988;38(1):172–80.

34) Williamson DF, Parker RA, Kendrick JS. The box plot: a simple visual method to interpret data. Ann Intern Med. 1989;110(11):916–21.

35) Jarrell SB. Basic Statistics (Special pre-publication ed.). Dubuque, Iowa Wm C Brown Pub. 1994;492.

36) Utts JM. Seeing through statistics. Cengage Learning; 2014.

37) Elliott P, Wartenberg D, Marshall RJ, Rosli NM, Shah SA, Mahmood MI, et al. A review of methods for the statistical analysis of spatial patterns of disease. J R Stat Soc Ser A (Statistics Soc. 2021;154(1):998–1006.

38) Nguyen TT, Vu TD. Use of hot spot analysis to detect underground coal fires from landsat-8 TIRS data: A case study in the Khanh Hoa coal field, North-East of Vietnam. Environ Nat Resour J. 2019;17(3).

39) Murad A, Khashoggi BF. Using GIS for disease mapping and clustering in Jeddah, Saudi Arabia. ISPRS Int J Geo-Information. 2020;9(5):328.

40) Gao S, Mioc D, Anton F, Yi X, Coleman DJ. Online GIS services for mapping and sharing disease information. Int J Health Geogr. 2008;7:1–12.

41) Rican S, Salem G. Mapping disease. A companion to Heal Med Geogr. 2009;14:96.

42) Vu D-T, Nguyen T-T. Spatial pattern of land surface temperatures and its relation to

Jilin Daxue Xuebao (Gongxueban)/Journal of Jilin University (Engineering and Technology Edition)
ISSN: 1671-5497
E-Publication: Online Open Access
Vol: 42 Issue: 10-2023
DOI: 10.5281/zenodo.10060151

underground coal fires in the Khanh Hoa Coal Field, North-East of Vietnam. Arab J Geosci. 2021;14(3).

43) Fecht D, Hansell AL, Morley D, Dajnak D, Vienneau D, Beevers S, et al. Spatial and temporal associations of road traffic noise and air pollution in London: Implications for epidemiological studies. Environ Int. 2016;88:235–42.

44) Kulldorff M, Feuer EJ, Miller BA, Freedma LS. Breast cancer clusters in the northeast United States: a geographic analysis. Am J Epidemiol. 1997;146(2):161–70.

45) Hoang A, Nguyen T. Identifying Spatio-Temporal Clustering of the COVID-19 Patterns Using Spatial Statistics: Case Studies of Four Waves in Vietnam. Int J Appl Geospatial Res. 2022;13(1):1–15.

46) Vu D-T, Nguyen T-T, Hoang A-H. Spatial clustering analysis of the COVID-19 pandemic: A case study of the fourth wave in Vietnam. Geogr Environ Sustain. 2021;14(4).

47) Cliff AD, Ord JK. Spatial processes: models & applications. (No Title). 1981;

48) Mitchell A. The ESRI guide to GIS analysis: geographic patterns & relationships. Vol. 1. ESRI, Inc.; 1999.

49) Anselin L, Syabri I, Kho Y. GeoDa: an introduction to spatial data analysis. In: Handbook of applied spatial analysis: Software tools, methods and applications. Springer; 2009. p. 73–89.